A Connectionist Computational Architecture based on an Optical Thin-Film Model

Martin Purvis and Xiaodong Li
Computer and Information Science
University of Otago
Dunedin, New Zealand
tel: 64 (03) 479-8318
email: purvis@otago.ac.nz

Abstract

A novel connectionist architecture that differs from conventional architectures based on the neuroanatomy of biological organisms is described. The proposed scheme is based on the model of multilayered optical thin-films, with the thicknesses of the individual thin-film layers serving as adjustable 'weights' for the training. A discussion of training techniques for this model and some sample simulation calculations in the area of patten recognition are presented. These results are shown to compare with results when the same training data are used in connection with a feed-forward neural network with back propagation training. A physical realization of this architecture could largely take advantage of existing optical thin-film deposition technology.

1 Introduction

Although connectionism has taken its inspiration from the neuroanatomy of biological organisms, the essence of this form of computation does not require strict adherence to the biological exemplar. What it fundamentally implies is simply an interconnected set of parallel distributed processing elements with nonlinear transfer functions between the elements [1,2,3]. Thus connectionist architectures that differ significantly from the biological model may still exhibit interesting computational properties and may be worthy of consideration. In this paper we describe an alternative connectionist architecture that takes its inspiration from the technology of optical multilayer thin-films (see Figure 1) and which we will refer to as the Optical Thin-Film Model (OTFM).

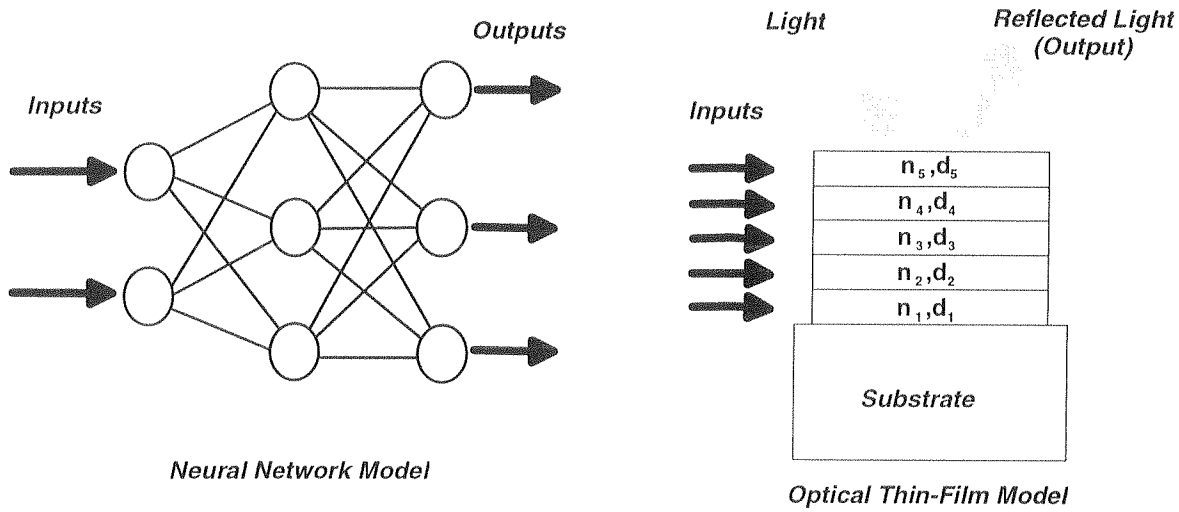

Figure 1. Neural network and optical thin-film connectionist models.

Section 2 provides a brief background on the optical properties of thin-film multilayers. Section 3 describes how information could be encoded into appropriate optical signals so that connectionist computations could be performed. Section 4 describes the computational method used to train a simulated thin-film multilayer with a training set. Section 5 presents some sample experimental calculations with this simulation model and compares the results to those performed with a conventional neural net architecture. Section 6 discusses the possibility of a physical realisation of this optical thin-film architecture for connectionist computations.

2 Optical thin-films

We will first consider the optical properties of a single (ideal) thin-film and then go on to consider the case when there are several contiguous thin-films.

2.1 Reflection and transmission coefficients for a single, isolated layer.

We assume the material of the thin-film is uniform, mostly transparent, and non-dispersive and can be characterised by a single index of refraction, ***n***. Its physical configuration can be represented by a plane parallel plate existing in a medium, such as a vacuum, whose index of refraction is equal to 1.0 (Figure 2). When a light beam of a single wavelength is incident on such a plane parallel plate, the beam is split into two parts -- a reflected beam and a transmitted

(refracted) beam that enters the material. The respective angles and magnitudes of these two newly created beams are determined by (a) the polarization and wavelength of the incident light beam, (b) the angle of incidence of the beam with the plate (thin-film) and (c) the index of refraction of the plate material [4,5]. Figure 2 shows the amplitudes of these individual light beam components, with the incident beam shown (on the left) to have an initial amplitude of a. The amplitude of the reflected beam component (on the left of the figure) is reduced by the reflection coefficient, r, and the amplitude of the transmitted component of the beam is reduced by a transmission coefficient, t. When the transmitted beam inside the plate material reaches the other surface, it is again split up into a reflected beam attenuated by the reflection coefficient r, and a refracted beam attenuated by a second transmission coefficient, t', associated with light that passes from a refractive material back into the vacuum. As can be seen in the figure, the light beam component inside the plate continues to undergo reflections and refractions, such that there are a number of reflected beams (ar, $atrt'$, atr^3t', atr^5t', atr^7t', . . .) and transmitted beams (att', atr^2t', atr^4t', atr^6t', . . .) that come off the top and bottom of the plate.

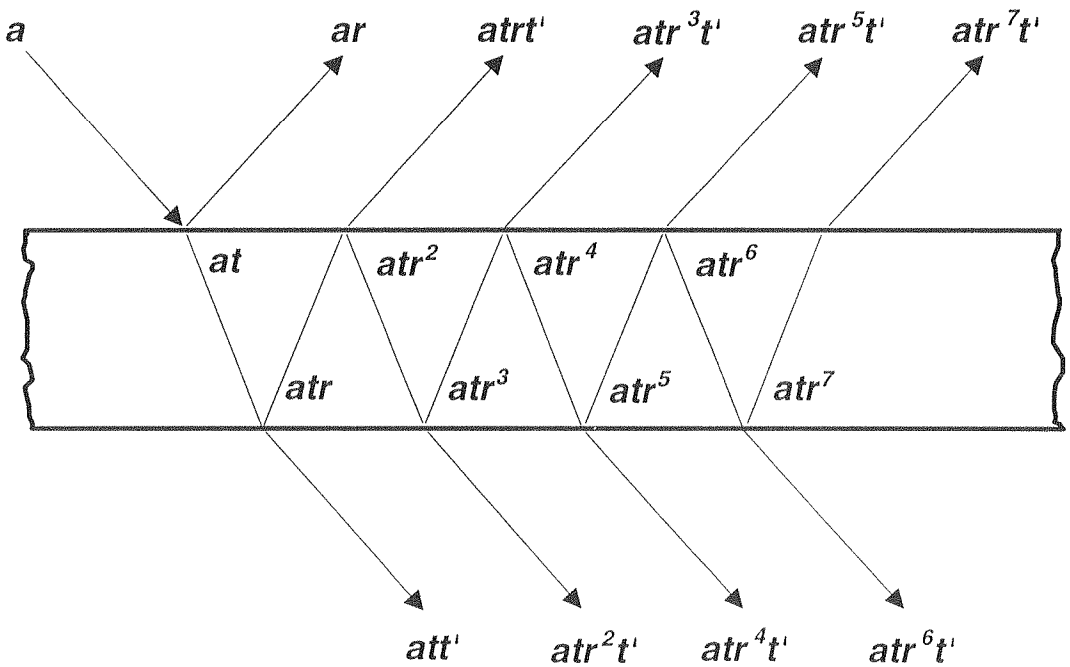

Figure 2. Multiple reflections and refractions in a thin-film.

Since the reflected beams, ar, $atrt$, atr^3t' atr^5t', etc., are waves, they differ from each other in both amplitude and phase, and the overall reflection of the light beam off the plate will be determined

by the multiple-beam interference of this infinite series of reflected component waves [5]. Algebraic expressions for the overall reflection and transmission coefficients (Eqs. (4) and (5), below) can be derived in a self-consistent manner if the simplifying assumption is made that the incident beam is perpendicular to the surface of the plate (thereby eliminating the polarization as a factor).

The parameters used in these expressions are characterised in Figure 3.

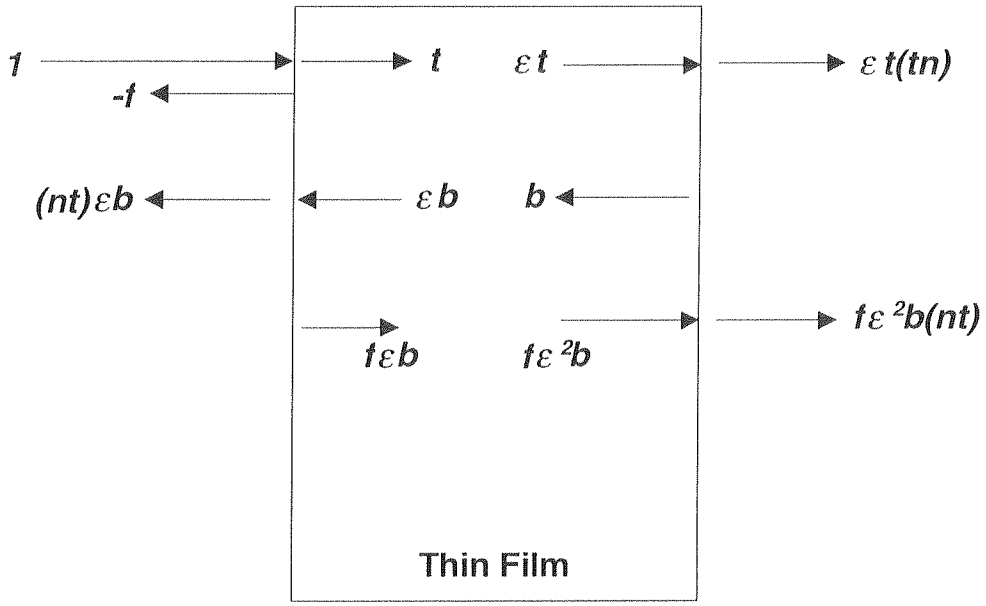

Figure 3. A single thin-film with light incident (*1*) on the left.

A monochromatic light beam (*1* in Figure 3) with wavelength λ is incident on the left side and, to simplify the presentation, is taken to have an electric field vector[1] amplitude normalized to 1. At the left surface of the thin-film, the incident beam is split into a transmitted component and reflected component with amplitudes $-f$ and t, respectively, where

$$f = \frac{(\tilde{n} - 1)}{(\tilde{n} + 1)} \qquad \text{and} \qquad t = \frac{2}{(\tilde{n} + 1)} \qquad (1)$$

$\tilde{n}$ is the complex refractive index of the thin-film, and $\tilde{n} = n + ik$, where n is the ordinary index

[1]The light wave also has a magnetic field vector component, but it is sufficient to consider only the electric field vector here. The phase of the wave is customarily incorporated into the description by representing the component as having a complex amplitude.

of refraction and k is the attenuation coefficient. The transmitted beam component with amplitude t now undergoes a phase shift as it travels a distance d (the thickness of the film) up to the right hand surface, so that its phase shifted amplitude is εt, where

$$\varepsilon = e^{i\frac{2\pi\tilde{n}d}{\lambda}} \tag{2}$$

At the right-hand boundary the beam is again split up into transmitted and reflected components. The transmitted component that emerges on the right has an amplitude of $\varepsilon t(tn)$. Since the reflected component is one of an infinite series of reflected components at this interface, they can be lumped together to represent the interference combination of all of the reflected components by b in Figure 3; εb is the phase shifted result of this leftward-travelling wave at the inside left-hand surface of the film. At the left hand surface, the wave with amplitude εb is split into a refracted (transmitted) component with amplitude $nt\varepsilon b$ and a reflected component travelling back to the right with amplitude $f\varepsilon b$. At the right-hand surface, the phase-shifted rightward travelling wave, here with amplitude $f\varepsilon^2 b$, is also split into two components: a reflected component already accounted for by b and a transmitted component with amplitude $f\varepsilon^2 bnt$.

Expressions for the reflection and transmission coefficients of the thin-film can now be taken directly from Figure 3:

$$r_f = -f + nt\varepsilon b \qquad \text{and} \qquad t_f = (\varepsilon t + f\varepsilon^2 b)nt \tag{3}$$

When these two equations are solved for the unknown b, the complex reflection and transmission coefficients can be given in terms of the refractive index and thickness of the film and the wavelength of the incident light (using expressions 1 and 2):

$$r_f = \frac{-f + \varepsilon^2 f}{1 - f^2\varepsilon^2} \tag{4}$$

and

$$t_f = \frac{\varepsilon(1 - f^2)}{1 - f^2\varepsilon^2} \tag{5}$$

2.2 Reflection and transmission coefficients for a multilayer thin-film structure

The reflection and transmission coefficients for a *multilayer* thin-film structure are obtained by means of a recursive approach. Assume several thin-films with different refractive indices have been successively deposited on top of a substrate material to form a multilayer thin-film stack (Figure 4). Let r_s denote the complex reflection coefficient at the outer surface of the thin-film structure, and let t_s denote the transmission coefficient in the substrate (output medium) at the last boundary surface. The values of these coefficients will depend on the refractive indices and thicknesses of all the films in the structure, the refractive index of the output medium, and the wavelength of light.

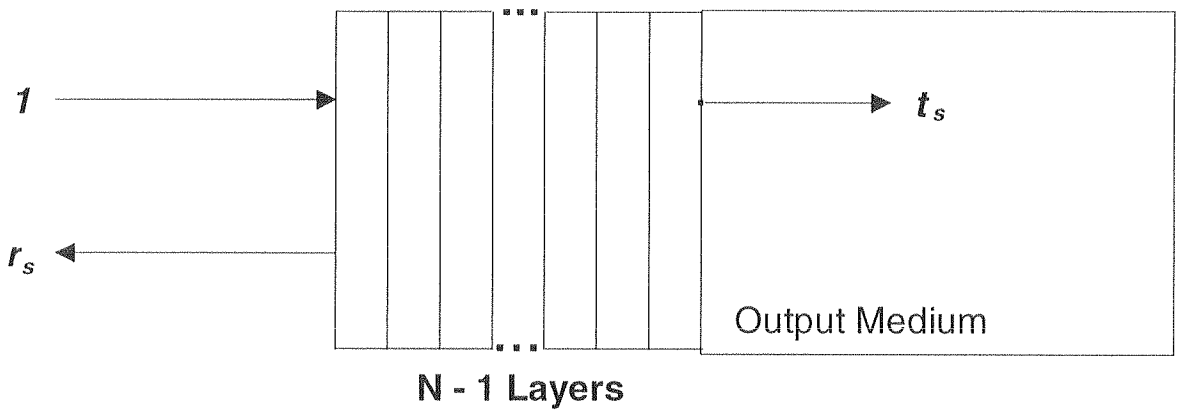

Figure 4. A multilayer stack of N - 1 thin-films deposited on a substrate (output medium).

Imagine an additional thin-film layer that is brought up to an existing thin-film multilayer structure of *N-1* layers whose values of r_s and t_s are already known (Figure 5). The additional thin-film layer is going to be the *Nth* layer and has a refractive index of $\tilde{n}_N = n_N + ik_N$. The distance between the *Nth* layer and the *N-1* layer substructure will be zero, but the layers are shown separated in Figure 5 for the purposes of explanation.

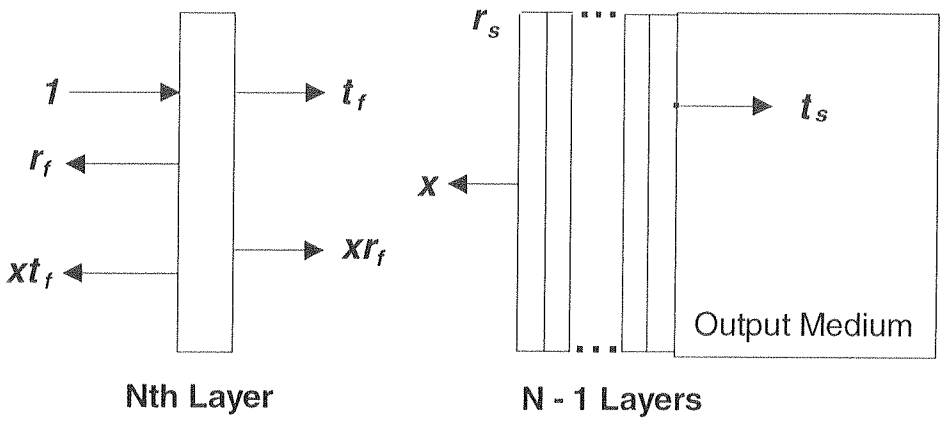

Figure 5. An additional thin-film layer is brought up to a multilayer structure of N-1 layers.

Again, the incident light on the left is taken to have a normalized amplitude value of 1. Eqs. (4) and (5) are used to determine r_f and t_f for the *Nth* layer. Since the light incident on the *N-1* layer substructure does not have an amplitude of 1, the amplitude of light reflected off its front surface is not its reflection coefficient r_s, but some other value, which we take to be x. This reflected light with amplitude x is partially reflected by the *Nth* layer back towards the substructure and partially transmitted through the *Nth* layer out to the left, and these components have amplitudes of xr_f and xt_f, respectively. The *N-1* layer substructure has a reflection coefficient of r_s, and self-consistency requires that the following relations hold:

$$\begin{aligned} r &= r_f + t_f x \\ t &= (t_f + r_f x)t_s \\ x &= (t_f + r_f x)r_s \end{aligned} \tag{6}$$

Eliminating x from the above yields the following expressions for r and t:

$$r = \frac{r_f + (t_f^2 - r_f^2)r_s}{1 - r_f r_s} \tag{7}$$

and

$$t = \frac{t_f t_s}{1 - r_f r_s} \tag{8}$$

r and t are the reflection and transmission coefficients for a N layer thin-film stack and r_s and t_s are the corresponding coefficients for a N-1 layer thin-film stack. Relabelling these terms so that they correspond to the number of layers in the film stack and substituting in the expressions for r_f and t_f from equations (4) and (5) yields the following recursive expressions for calculating the thin-film stack reflection and transmission coefficients:

$$r_N = \frac{-f_N(1 - \varepsilon_N^2) + (\varepsilon_n^2 - f_n^2) r_{N-1}}{(1 - f_N^2 \varepsilon_N^2) + f_N(1 - \varepsilon_N^2) r_{N-1}} \tag{9}$$

and

$$t_N = \frac{\tilde{n}_N \tau_N^2 \varepsilon_N}{(1 - f_N^2 \varepsilon_N^2) + f_N(1 - \varepsilon_N^2) r_{N-1}} \tag{10}$$

with

$$f_N = \frac{\tilde{n}_N - 1}{\tilde{n}_N + 1}, \quad \tau_N = \frac{2}{\tilde{n}_N + 1} \quad \text{and} \quad \varepsilon_N = e^{i\frac{2\pi \tilde{n}_N d_N}{\lambda}} \tag{11}$$

The recursive expressions shown in equations (9) and (10) provide the means for computing the reflection and transmission coefficients for a thin-film stack of any number of layers. It is these highly nonlinear expressions that form the basis for the connectionist computations to follow. The optical reflectance and transmittance, which are what is ordinarily obtained from optical

measurements of thin-film stacks, are directly derived from the reflection and transmission coefficients:

$$R(\lambda) = |r(\lambda)|^2 \qquad \text{and} \qquad T(\lambda) = |t(\lambda)|^2 \qquad (12)$$

3 Encoding information in the optical thin-film model

Expressions (9), (10), and (11) describe the reflection and transmission coefficients of a N-layered thin-film stack in terms of the N refractive index and thickness values of the layers and the optical wavelength of light. For computational purposes, these coefficients, with real and imaginary values always in the range of -1.0 to +1.0, may be considered to be a generalized output. It is also possible, by means of expressions (12), to use reflectance and transmittance as generalized outputs and thereby associate computations more directly with conventional optical measurements. Both of these approaches have been used in experiments reported in this paper. With these generalized outputs and for a specified range of optical wavelengths, virtually any desired spectral characteristic of these coefficients can be obtained by choosing a set of thin-film layers with appropriate values of thickness and refractive index [6,7].

There are several possible schemes for encoding input information to be used for computational purposed with this model [6]. The approach employed in this paper is to encode input into the indices of refraction of the various thin-film layers. Under this scheme if there are to be M input values for a computation, then there must be at least M thin-film layers available. As is shown in the next section, the thicknesses of the various layers are then used as adjustable 'weights' to obtain the desired output.

Figure 6 shows an example of this encoding scheme. A five-layer thin-film stack is shown, each layer characterized by its refractive index, n_i, and its thickness, d_i. For each layer i, one of the inputs is encoded into an appropriately scaled value of the refractive index $n_{\Delta i}$, and added to a base value of that layer's refractive index, n_{Bi}, (with $n_{\Delta i} << n_{Bi}$) to arrive at the layer's index value n_i. The values of n_{Bi} are kept large enough relative to the encoded incremental values, n_{Δ}, to

ensure that there is always a substantial variation of the refractive index n_i from layer to layer, irrespective of the value of the input for that layer. Note that it is not necessary for every layer of the stack to be used for input; a thin-film stack could be designed with some extra layers that are not used for encoding input.

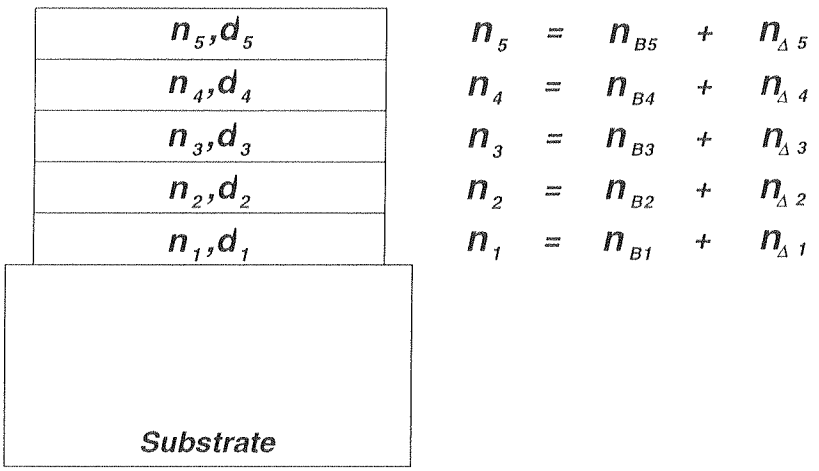

Figure 6. A thin-film stack with inputs encoded as incremental values of the refractive indices.

The thin-film stack provides output values of the reflection and transmission coefficients for each value of the optical wavelength. One can use a single wavelength for a computation, but it is often more effective to use multiple wavelengths in order to provide better discrimination among the various outputs. When multiple wavelengths are used, an indexing scheme must be set up that maps a desired computational output to a particular spectral response of the system over the wavelength range. Examples of this approach will be shown when sample calculations are presented in section 5.

4 Training with the optical thin-film architecture

The goal of training is to determine a set of appropriate layer thicknesses in the OTFM to satisfy the target optical specifications, and it can be viewed as supervised learning based on direct comparison of the model output with known correct answers [8]. The learning process proceeds until the model yields an acceptable output upon presentation of the appropriate input. The degree to which an output is acceptable can be measured by the value of a merit function, which, for example, can be taken to have the form:

$$M(x) = \sum_{k=1}^{m} (R_0(\lambda_k) - R(x,\lambda_k))^2 \qquad (13)$$

where x is the vector of design variables including parameters such as individual layer thicknesses, R_0 is the target reflectance at λ_k,, R is the computed value of reflectance at λ_k for a particular value of x, and m is the number of wavelengths. The goal of learning then is to achieve a suitably small value of the merit function, which corresponds to the cost function in a neural network. An alternative merit function can be taken to be:

$$M(x) = \sum_{k=1}^{m} |(r_0(\lambda_k) - r(x,\lambda_k)|^2 \qquad (14)$$

where r_0 is the target reflection coefficient at λ_k, and r is the complex reflection coefficient at λ_k for a particular x, so that the reflectance $R = |r|^2$. The advantage of this second formulation is that an extra variable (real and imaginary components of r_0 rather than just a real value R_0) can be specified for a target at a given wavelength, and hence it is possible to specify more tasks with fewer wavelengths. This can have the consequence of reducing the amount of computation involved. Since Eq. (13) corresponds to conventional optical measurements, it should be easier to implement in an optical realisation.

The training procedure is an iterative approach involving the following steps:

(1) Initialize the thickness and refractive index of each layer, and assign the initial best merit value $M_{Best} = \infty$. Specify the optical targets (here, for illustration, we use reflectance values) at each λ (wavelength).

(2) Repeat until the M_{Best} is sufficiently small (or until a specified number of iterations have been completed).

(2a) Vary the thicknesses of some layers using a search algorithm to find an optimal set of layer thicknesses.

(2b) Calculate R or r at each λ.

(2c) Calculate merit function M using either Eq. (13) or (14).

(2d) If $M < M_{Best}$, then assign the value of M to M_{Best} and update the thickness of each layer and other parameters necessary for the later calculations.

Training the optical thin-film multilayer involves searching for an appropriate OTFM configuration by observing the value of the merit function for each thickness combination. There are two factors that can make this search computationally expensive:

(1) Exhaustive search of all possible thickness combinations is prohibitive for a large number of layers. For instance, for a 10 layer model and assuming that 20 different thicknesses are evaluated for each layer, exhaustive search would require 20^{10} evaluations.

(2) If Eqs. (9) and (10) are used to compute the reflection and transmission coefficients of a multilayer, then whenever an individual layer thickness is altered, the reflection and transmission coefficients for each other layer would ordinarily have to be recalculated in order to determine the multilayer reflection and transmission coefficients.

Optimization procedures can be used to deal with both of these difficulties [9,10], and in the present work two optimization procedures are employed to provide more effective training. In order to prune the large search space, the "N-squared scan" approach [11] is used. Though it may miss out an optimal solution, the "N-squared scan" approach has been shown to be useful in practice [12]. To avoid reevaluating the optical performance of unaltered layers (difficulty 2, above) we have developed an algorithmic routine is used to short cut the calculation process of the multilayer reflectance, without relying on Eqs. (9) and (10) to compute the reflection and transmission coefficients for each layer repeatedly. This technique takes advantage of some intermediate elements of previous multilayer calculations that can be retained for subsequent use.

5 Experimental Calculations with the Optical Thin-Film Model

In this section the performance of the Optical Thin-Film Model is examined with respect to several widely studied data sets [2,8,13,14] and compared with the performance of a "conventional" connectionist learning algorithm, the multilayer perceptron with backpropagation training (labelled "BP" in the following).

5.1 Data Sets Used

Five different sets of data are used for experimental training and test: XOR, PARITY, PATTERN1, PATTERN2, and IRIS. The first four have binary values (either 1.0 or 0.0), but the fifth data set (IRIS) is continuous-valued. The XOR data set has four 2-bit binary numbers as inputs. The PARITY data set comprises 16 four-bit binary numbers for the inputs. For visual pattern recognition two examples on a 5 by 5 grid are covered: PATTERN1, comprising four distinct patterns, and PATTERN2, comprising eight distinct patterns. For both PATTERN1 and PATTERN2 input patterns containing errors are also presented to examine the degree to which the OTFM can, as other connectionist architectures, classify correctly and degrade gracefully in the presence of noise. The IRIS data set [15] concerns the classification of three different classes of iris plant and contains 150 samples divided into a training and a test data set.

5.2 Experimental Results

For each of the experiments illustrated here, the OTFM multilayer is assumed to be deposited on a substrate with a refractive index of 4.0 (corresponding to the refractive index of germanium in the microwave region of the spectrum) and the input medium is taken to have a refractive index of 1.0 (corresponding to air). As discussed in section 4, the output values of an OTFM stack can be chosen to be the complex-valued reflection and transmission coefficients or the real-valued reflectance and transmittance coefficients (absolute magnitudes of the complex-valued coefficients). Depending on what is chosen, either Eq. (13) or (14) above is used. For the XOR, PARITY, and PATTERN1 data sets the reflectance coefficient was the output parameter used, and the merit value was determined by expression (13). For the PATTERN2 and IRIS data sets the complex reflection coefficient was used as the output parameter, and the merit value was determined by expression (14).

For the BP model, the learning rate is typically set to 0.2, and the momentum is set to 0.1. The best training result is selected out of 5 trainings for each data set.

5.2.1 XOR: the XOR problem

The XOR problem involves training a system to reproduce the Boolean exclusive-or logical function and is the simplest case of the *N*-input parity problem. It is also perhaps the simplest classification problem that is not linearly separable. Table 1 shows that the desired computation (training target) is 1.0 if the first input is 0.0 and the second is 1.0 or if the first is 1.0 and the second is 0.0; otherwise the desired output is 0.0.

Inputs		Targets	OTFM (8 layers)	BP (2 hidden nodes)
0	0	0	0.100546	0.02760
0	1	1	0.813596	0.97010
1	0	1	0.728428	0.97008
1	1	0	0.195737	0.03752

Table 1. Training results on the XOR problem.

Layer	N	Thickness
1	1.2	1.278507
2	2.4	1.010522
3	1.2	2.427093
4	2.4	0.093837
5	1.2	0.798172
6	2.4	0.299938
7	1.2	0.797708
8	2.4	0.291884

Table 2. Optical description of a 8-layer OTFM for solving the XOR problem. "N" shows the initial refractive indices. "Thickness" shows a found thickness combination, which results in a solution of the XOR problem shown in Table 1.

An 8-layer OTFM (shown in Table 2) was used for training to solve the XOR problem. In each input row as shown in Table 1, two input bits were encoded into the refractive index of the first layer and second layers respectively (see section 3). The model was trained for an input light wavelength value of 4 μm. The refractive index scaling factor for the inputs (maximum value of $n_{\Delta i}$) was set to be 0.7 (see figure 6). Table 1 shows the result of this training. For a tolerance value of 0.3, the results in the "Reflectance" column are acceptable according to the "Target" column. Also shown in Table 1 are the results for a "BP" neural network with two nodes in the hidden layer. The training time for the OTFM in this case was approximately 4 minutes and for the BP model approximately 10 minutes.

5.2.2 PARITY: the parity problem

The parity problem examined here has 16 four-bit binary numbers and is frequently used for evaluating connectionist models because of its nonlinearity [8]. The desired output is 0.0 if the parity of the four-bit number is even, and 1.0 if the parity is odd.

Inputs				Targets	OTFM (25 layers)	BP (4 hidden nodes)
0	0	0	0	0	0.246310	0.02224
0	0	0	1	1	0.640190	0.99903
0	0	1	0	1	0.596955	0.99902
0	0	1	1	0	0.286317	0.00921
0	1	0	0	1	0.822227	0.99903
0	1	0	1	0	0.214709	0.00920
0	1	1	0	0	0.213929	0.00918
0	1	1	1	1	0.832500	0.96059
1	0	0	0	1	0.784272	0.99903
1	0	0	1	0	0.207857	0.00921
1	0	1	0	0	0.145810	0.00918
1	0	1	1	1	0.822444	0.96040
1	1	0	0	0	0.285641	0.00918
1	1	0	1	1	0.600092	0.96021
1	1	1	0	1	0.553203	0.96004
1	1	1	1	0	0.342155	0.08257

Table 3. Training result for solving the parity problem. If the tolerance is set to 0.5, the OTFM outputs are acceptable according to the targets required.

Table 3 shows the result of the OTFM training for solving the parity problem, using the PARITY data set. In this training, a 25-layer OTFM was used to obtain the desired reflectances at an wavelength of 4.4 μm. The refractive index scaling factor was set to be 0.5. Although the result of this training does not show the degree of precision obtained by a BP network trained with the same data set, the desired computation is obtained. For a tolerance setting of 0.45, the trained OTFM matches the target settings. The training times were approximately 18 minutes for this optical thin-film stack and apprxoimately 32 minutes for the BP network.

5.2.3 PATTERN1: recognition of four 5 X 5 grid patterns

Four 5 by 5 grid patterns were used for training in this experiment. As in the preceding two experiments, the reflectance was used as the OTFM output and expression (13) was used as the merit function for training. Figure 7 shows the four 5 by 5 grid patterns ('I', 'O', 'C', and 'X') that the model was trained to recognize.

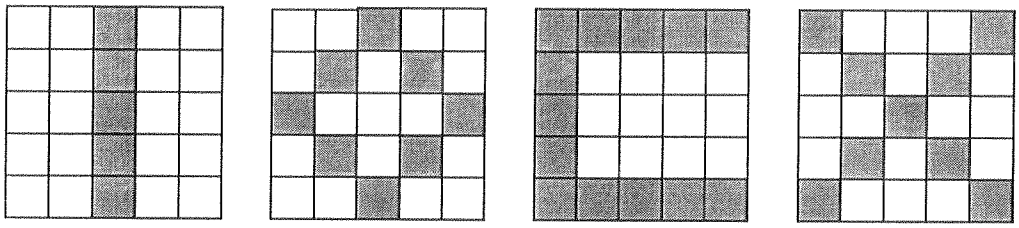

Figure 7. Four 5 by 5 grid patterns: 'I', 'O', 'C' and 'X'. A black square represents 1.0, and a blank square represents 0.0.

A multilayer film stack of 25 layers was trained for this recognition task. Each element in the input pattern ("pixel") represented either 1.0 (black) or 0.0 (blank) and was encoded into the refractive index of a given layer. Thus the 25 input values of the pattern were coded into the 25 individual layer refractive indices in the model. For each of these target input patterns, the OTFM was trained with respect to a set of target reflectances at 8 separate wavelengths, ranging from 10 μm to 12.8 μm. The 8 target reflectances were specified differently for each pattern as shown in Fig. 8. The goal was to train the model film stack to produce reflectances as close as possible to the target reflectances, so that after training it would be able to distinguish these patterns to a maximum degree.

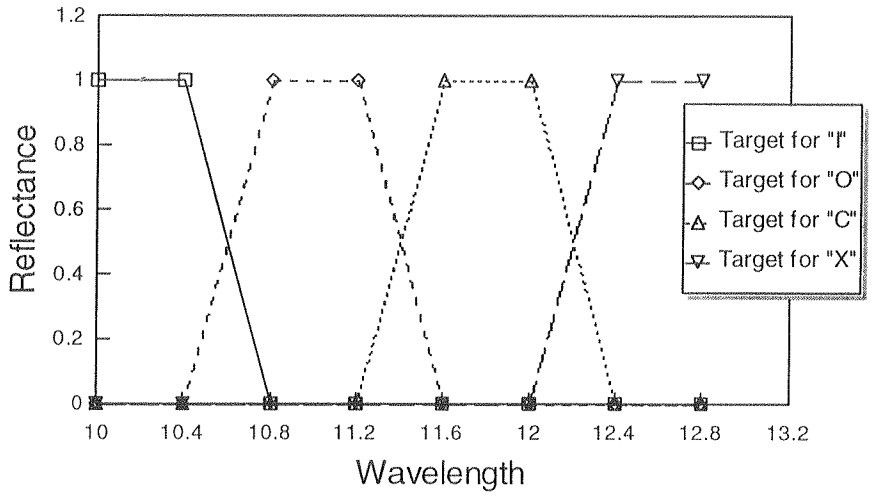

Figure 8. Training targets for four different patterns specified over wavelengths ranging from 10 to 12.8μm.

The results of this training can be seen in Figure 9, where it can be seen that the trained OTFM stack produced high and low values of reflectance approximately corresponding to the target values.

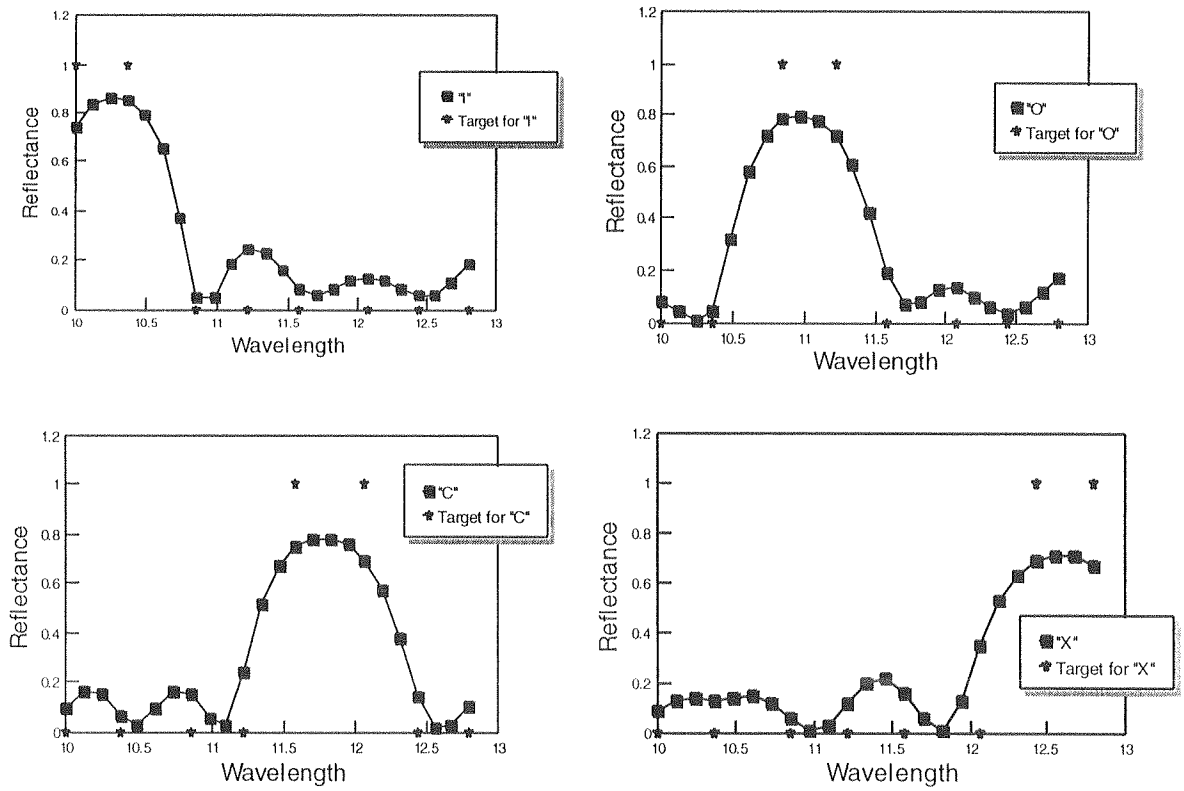

Figure 9. Plots of OTFM training results for 'I', 'O', 'C', and 'X'.

Although the target values were not achieved precisely, the output reflectance spectra easily distinguish the four patterns of Figure 7.

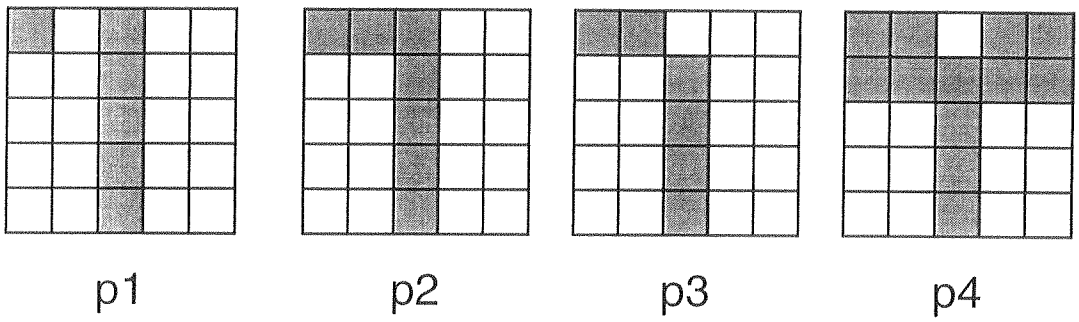

Figure 10. Four noisy versions of pattern "I".

To examine the response of the OTFM in the presence of noise, four noisy versions of pattern 'I', p1, p2, p3 and p4 were tested on the trained model (Figure 10). In these four patterns, the majority of black and blank digits of the pattern 'I' remain unchanged. Noise is added to the pattern by changing some the original pixels of 'I' from black to blank or from blank to black, with noise increasing gradually from p1 to p4: the pattern p4 is considered as the poorest pattern of

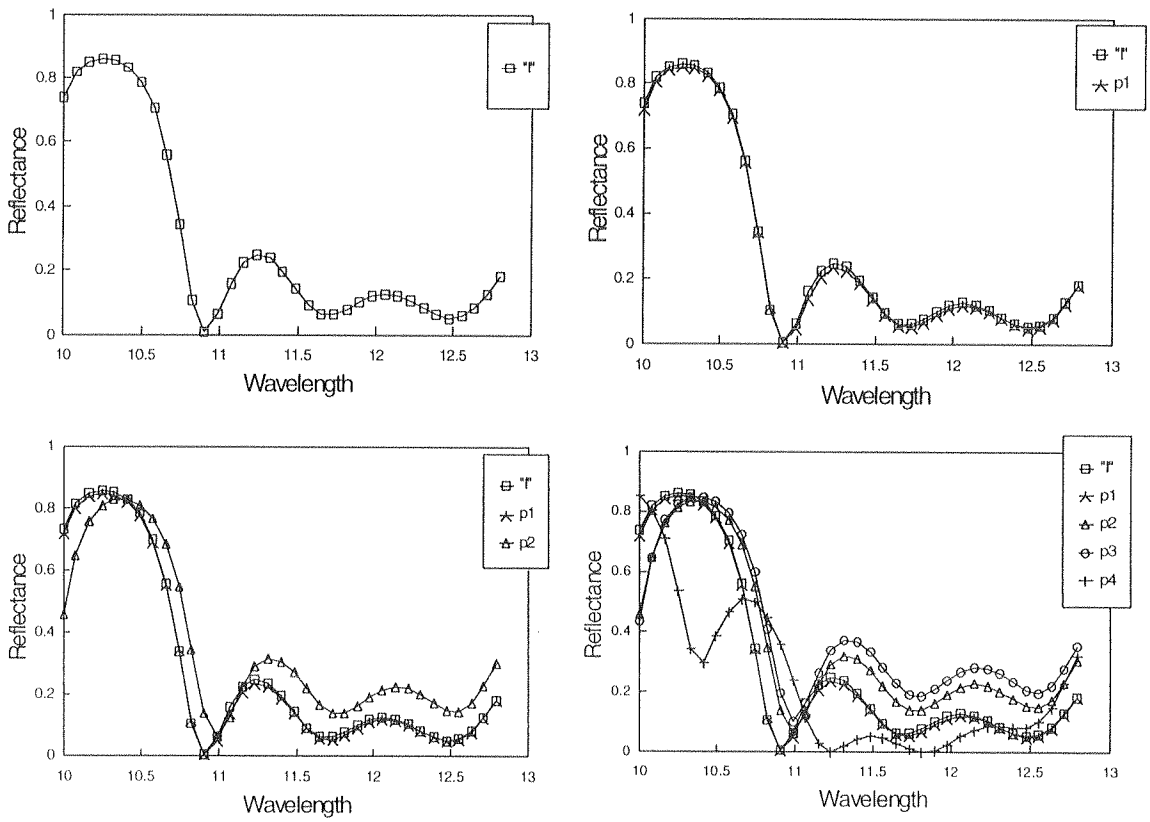

Figure 11. Plots of the testing results on 'I' and on its noisy versions p1, p2, p3, and p4.

'I'. The intent is to examine the manner in which performance degrades in the OTFM.

Depending on the tolerance required, noisy patterns of 'I', p1, p2, p3 and p4 can be classified as 'I' or a "wrong" pattern. For example for a low tolerance, only p1 is qualified to be 'I', and p2, p3 and p4 are all classified as "wrong" patterns. As shown in Figure 11, as the noise increases from p1 to p4, the resulting reflectance curve becomes more distant from the target reflectance curve, indicating that the system degrades gracefully with increasing noise. Even for p4, its curve can still be seen as closer to 'I', compared with the reflectance curves of 'O', 'C' and 'X' in Figure 8.

The OTFM training for this experiment took 16 minutes, while a BP network trained with PATTERN1 took 2 minutes to complete a satisfying training. However if fewer wavelengths can be used for OTFM, the training time can be reduced substantially.

To reduce training time, the same OTFM stack with the 4 patterns of PATTERN1 was trained by using complex reflection coefficients specified at only two different target wavelengths and using the merit function of Eq. (14) was also performed. Compared with the first training method used with PATTERN1, the performance of the OTFM improved: a lower error rate was obtained, and the training time was much shorter (since only two wavelengths were necessary). A similar experiment with this approach, in which 8 patterns were used (PATTERN2 data set) for training, is described in the following section.

5.3.4 PATTERN2: recognition of eight 5 X 5 grid patterns.

For the training of a pattern recognition problem involving 8 patterns, a more flexible approach is adopted by using the merit function Eq. (14). The complex reflection coefficient of a film stack can be represented as the vector sum of its real and imaginary parts, $r = \mathrm{Re}(r) + i\mathrm{Im}(r)$ and similarly the target reflection coefficient as $r_0 = \mathrm{Re}(r_0) + \mathrm{iIm}(r_0)$. Then rather than training the model by comparing R_0 and R, the training can be performed by comparing $\mathrm{Re}(r_0)$ with $\mathrm{Re}(r)$ and $\mathrm{Im}(r_0)$ with $\mathrm{Im}(r)$ directly. Since there are now two comparisons made for each wavelength value, the number of wavelengths needed in the computation is reduced and a computational saving results. This approach is illustrated here with a 8 pattern recognitions problem. The four patterns shown in Figure 7 were again used here, plus another four patterns shown in Fig. 12.

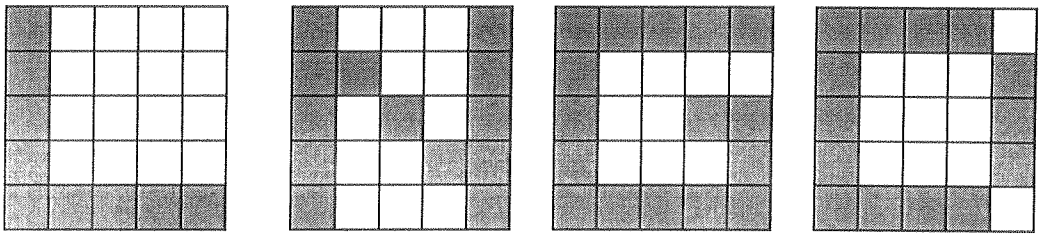

Figure 12. The additional four patterns used in the PATTERN2 data set.

A 25-layer stack was also used for this 8-pattern recognition experiment, and it was trained at a single wavelength of 8 μm. The specified target reflection coefficients for patterns 'I', 'O', 'C', 'X', 'L', 'N', 'G' and 'D' were distributed evenly around the outside of the unit circle of the complex plane and are shown in Figure 13. Any other points within the circle could have been chosen as target points, and it is a subject of further research to determine how best to distribute target points on the complex plane.

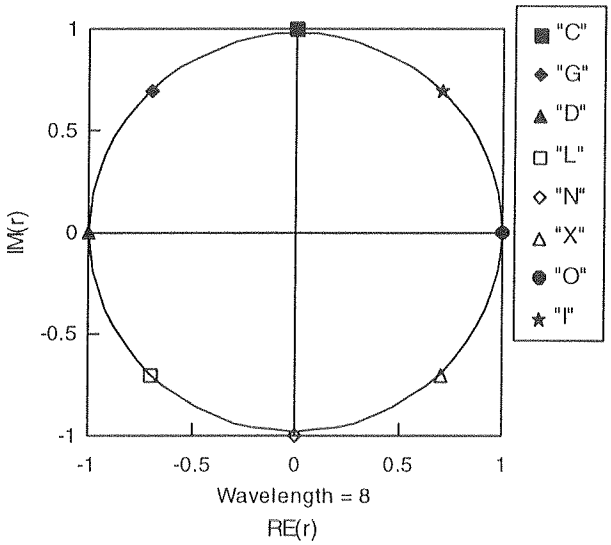

Figure 13. Targets specified for the 8 patterns of Figures 6 and 11.

After training the 25-layer stack for the specified targets, the stack yielded the reflection coefficients for the 8 patterns shown in Figure 14. Each of the resulting reflection coefficient points is the closest point to its corresponding. When a new input pattern is presented to the film stack, the distance to the nearest target reflection coefficient can be calculated to determine which pattern is 'closest' to the input pattern.

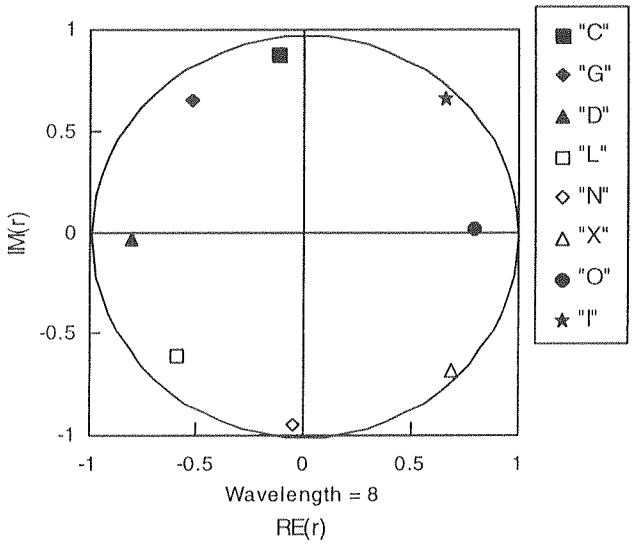

Figure 14. Training result for the 8 pattern recognition problem

In order to examine the trained model's response to noise, noisy versions of the pattern 'I' were also employed (Figure 14). As shown in Figure 15, additional pixels of noise have been added to the 'I' pattern to create the alternative patterns, p1, p2, and p3.

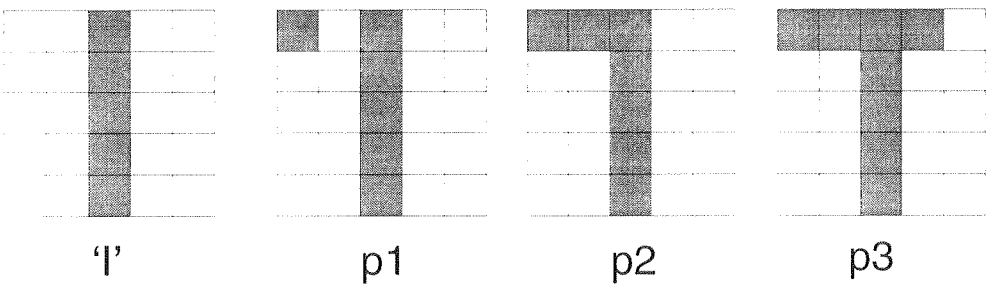

Figure 15. Noisy increasing steadily from 'I', p1, p2 and p3.

The result of applying these input patterns to the trained stack are shown in Figure 16: as noise increases the resulting reflection coefficient points move away from the reflection coefficient of the original 'I' pattern point. Thus the model film stack degrades gracefully with the addition of noise to the inputs.

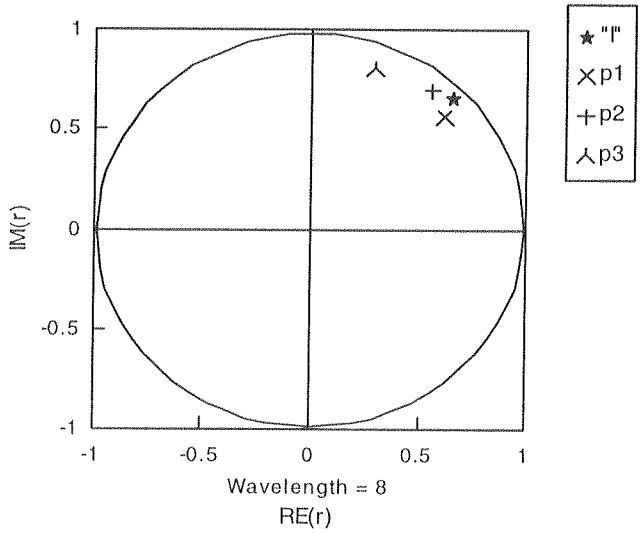

Figure 16. Result of noisy versions of 'I' (Figure 14) applied to the trained film stack (Figure 13).

5.3.5 IRIS: classification and generalization with the iris data set.

The iris data was first used by Fisher [16], and is still frequently used today as the standard discriminant analysis example [13]. The data set is used to discriminate three classes of iris using four continuous-valued features for each case. There are 150 cases, with 50 instances for each class. One class of the data is linearly separable from the other two, while those other two are not linearly separable from each other.

Each of the four features for the iris data set has a different range of values, so a separate scaling factor, Δ, was used for each feature, which was multiplied by the corresponding input value and the produce then added to the base value of the layer refractive index. The Δ scaling factors used for this experiment were 0.03, 0.08, 0.03, and 0.04 for the respective iris data features (*sepal length*, *sepal width*, *petal length* and *petal width*).

The training approach was the same as that used for the 8 grid pattern recognition experiment (using Merit function Eq. (14)), but 3 wavelengths were used for training on each pattern. The additional wavelengths were used to assist in the discrimination of the 2nd and 3rd iris classes, which are not linearly separable. The thin-film stack consisted of four layers, and training was carried out over wavelength values of 5.0 μm, 5.3 μm, and 5.6 μm. The target reflection coefficients (real and imaginary components) were {0.2, 0.2}, {0.3, 0.3} and {0.4, 0.4} for class 1, and {-0.5, 0.1}, {-0.4, 0.3} and {-0.3, 0.4} for class 2, and {0.1, -0.5}, {0.3, -0.4} and {0.4, -0.3} for class 3, as shown in Fig. 17.

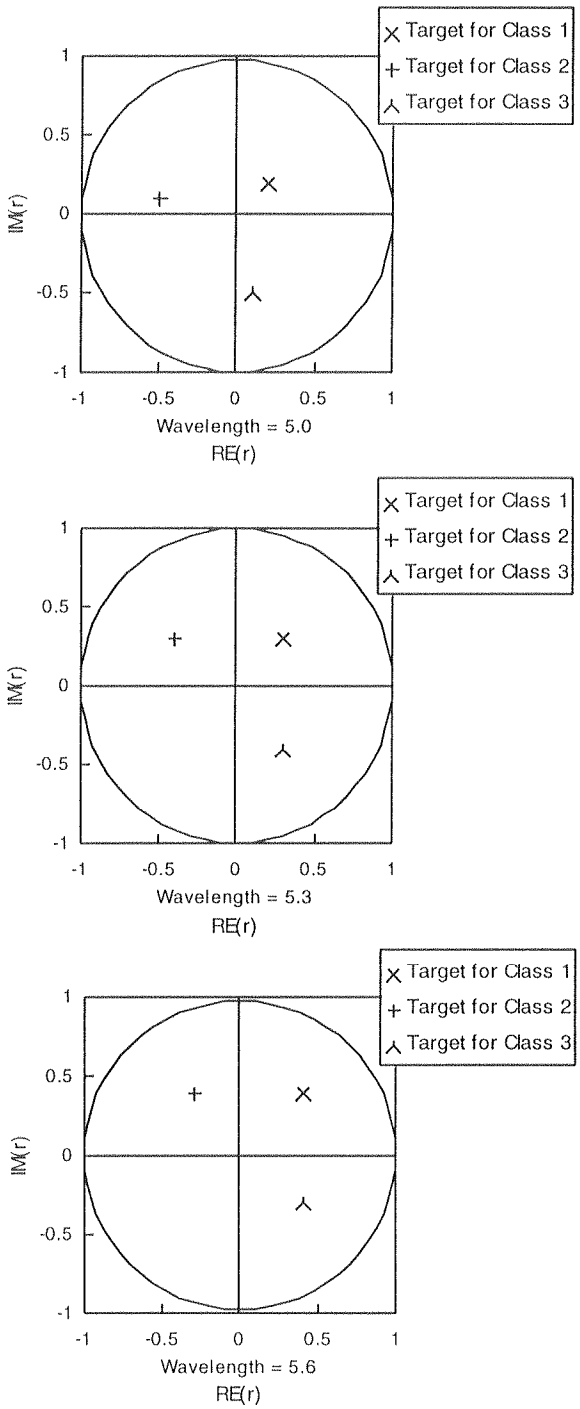

Figure 17. Target reflection coefficient points for IRIS classification at three wavelengths.

After the film stack was trained with 120 examples from the IRIS data set, it was tested with 30 novel test examples. A forced classification approach was employed that first takes the average

value of all the points for each training class at 3 different wavelengths. During testing this value is compared with the actual output; the one having the minimum difference is chosen as the classified type. Figure 18 shows the test results at the three wavelengths.

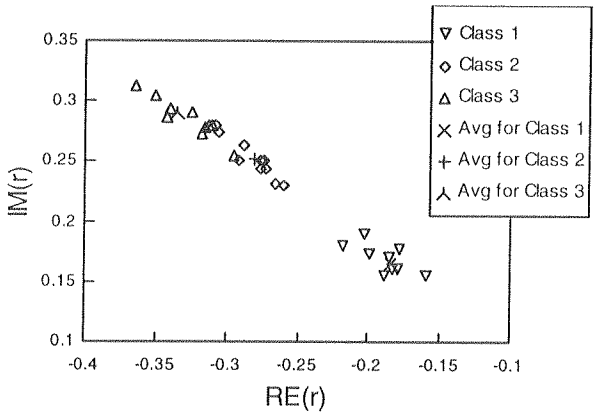

(a) Test results at wavelength = 5.0 μm

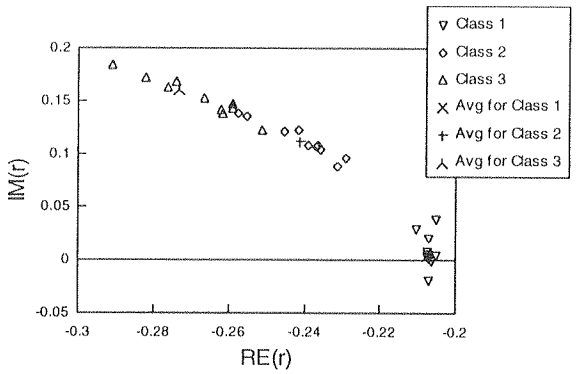

(b) Test results at wavelength = 5.3 μm

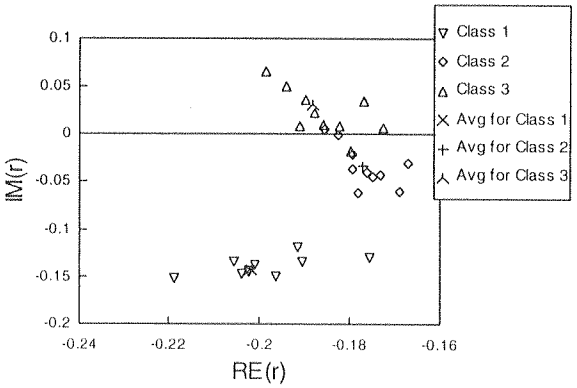

(c) Test results at wavelength = 5.6 μm

Figure 18. Test results on 30 IRIS examples.

The OTFM stack classified 28 out of the 30 test examples correctly in this experiment. When all 150 elements of the IRIS data set were presented, 5 were classified incorrectly. These results are comparable to neural network calculations that have been used in connection with the IRIS data set [13].

6 Conclusions

Connectionist models can be used to provide nonlinear mappings between their inputs and outputs. Neural networks achieve this mapping by adjusting the weights of connections among the processing units. The OTFM has a novel connectionist architecture whereby the thickness of each thin-film layer can be considered to be such an adjustable weighted connection. By searching for a set of appropriate thicknesses of individual layers, the goal of learning the association between the input and the output can be eventually achieved.

An optical realization of this architecture would offer the possibility of more or less instantaneous evaluations of the (trained) thin-film stack. Also, because optical beams at ordinary intensities do not interfere with each other, the architecture could support the simultaneous evaluation of multiple signals. The manner in which input is encoded into the thin-film architecture, however, would require adjustments to the refractive indices of the optical materials. Such variation of refractive index can be achieved for some materials by means of elastooptic, electrooptic, and magnetooptic effects [17], but the effects are often relatively small. An another approach could involve the use of gradient index optics, which are usually associated with fiber-optics, but which have also been deposited in the form of thin-films [18,19]. These materials have a refractive index that varies from point to point within the medium. By using such materials in thin-film multilayers, it would seem feasible that variable refractive index values could be achieved by physically redirecting a laser beam to the multilayer at different spots on the surface.

A more flexible approach would be to employ the Herpin equivalent index concept [20,21] as outlined by Dobrowolski and Piotrowski [22]. The Herpin equivalent index method can be used when there is a need to prepare a film with refractive index n, $n_L < n < n_H$ that does not correspond to that of any known material. The equivalent effect of such a film can be achieved

for a given optical wavelength by a suitable three-layer combination consisting of materials with indices n_L and n_H. This means that it is always possible to duplicate the performance of any multilayer system consisting of many different materials by one consisting of only the lowest and highest refractive-index materials from the original system, since one can always substitute any layer from the original system by a three-layer Herpin equivalent. Although the Herpin equivalent index is defined for a single wavelength, Dobrowolski and Piotrowski show how this approach can be used effectively for a thin-film multilayer over a range of wavelengths, as long as the range is not too great. Although this approach involves the introduction of additional thin-films and thus requires greater computation, it appears to offer the greatest flexibility for physical implementations of the optical thin-film multilayer connectionist architecture.

The observation that alternative distributed nonlinear architectures may have attractive computational properties has been made by several authors, for example Serra and Zanarini [23]. We are exploring one such architecture based on the technology of optical thin-film multilayers, which is of interest both for its novel computational properties and for the possibility of practical realizations in terms of optical systems.

References

[1] T. Khanna, *Foundations of Neural Networks,* (1990) Addison-Wesley, New York.

[2] D. E. Rumelhart, G. E. Hinton, and R. J. Williams, "Learning Internal Representations by Error Propagation." chapter 8 in D. E. Rumelhart, J. L. McClelland, *Parallel Distributed Processing*, vol. 1, (1986), The MIT Press, Cambridge, MA.

[3] S. C. Shapiro (*ed.*), *The Encycolopedia of Artificial Intelligenge, vol 1*, (1987) John Wiley & Sons, New York.

[4] F. A. Jenkens and H. E. White, *Fundamental of Optics,* (1976) McGraw-Hill, New York.

[5] M. Born and E. Wolf, *Principles of Optics*, (1980) Pergamon, New York.

[6] M. K. Purvis and Li X., "Connectionist Computations Based on an Optical Thin-Film Model", *Proceedings of the First New Zealand International Two-Stream Conference on Artificial Neural Networks and Expert Systems*, (1993) IEEE Computer Society Press, Los Alamitos, CA., pp. 130-133.

[7] M. K. Purvis, and X. Li, "Connectionist Learning Using an Optical Thin-Film Model", in *Proceedings of the Second New Zealand International Two-Stream Conference on Artificial Neural Networks and Expert Systems*, (1995) IEEE Computer Society Press, Los Alamitos, CA, pp. 63-66.

[8] J. Hertz, A. Krogh, and R. G. Palmer, *Introduction to the Theory of Neural Computation*, Redwood City, CA (1991) Addison-Wesley Publishing Company, Reading, MA.

[9] J. A. Dobrowolski, and R. A. Kemp, "Refinement of Optical Multilayer Systems with Different Optimization Procedures," *Applied Optics*, (1990) **29**: 2876-2893.

[10] W. E. Case, "New Synthesis Method for Optical Thin-Film Coatings," *Applied Optics*, (1983) **22**(24): 4111-4117.

[11] H. M. Liddell, *Computer-aided Techniques for the Design of Multilayer Filters*, (1981) Adam Hilger, Bristol.

[12] H. A. MacLeod, W. E. Case, and M. K. Purvis, "Design of a Vanadium Dioxide Switchable Coating", in *Topical Meeting on Optical Interference Coatings*, Opt. Soc. of Am., 1984.

[13] S. M. Weiss, and I. Kapouleas, "An Empirical Comparison of Pattern Recognition, Neural Nets, and Machine Learning Classification Methods," *Proceedings of the 11th International Joint Conference on Artificial Intelligence*, (1989) Detroit, pp. 781-787.

[14] B. D. Ripley, "Statistical Aspects of Neural Networks" in *Networks and Chaos -- Statistical and Probabilistic Aspects*, (1993) Chapman and Hall, London, pp. 40-123.

[15] E. Anderson, "The Irises of the Gaspe Peninsula", *Bulletin of the American Iris Society*, (1935) vol 59 , pp. 2-5.

[16] R. Fisher, "The Use of Multiple Measurements in Taxonomic Problems, *Ann. Eugenics*, (1936) **7**:179-188.

[17] L. Levi, *Applied Optics*, Vol II, (1980) John Wiley, New York.

[18] E. W. Marchand, *Gradient Index Optics*, (1978), Academic Press, New York.

[19] H. Fabricius, *Applied Optics*, **31**:25 (1992), pp. 5191-5196, 5216-5220.

[20] A. Herpin, *C. R. Acad. Sci*, (1947) **225**:182.

[21] L. I. Epstein, *J. Opt. Soc. Am*, (1952) **42**:806.

[22] J. A. Dobrowolski and S. H. C. Piotrowski, "Refractive Index as a Variable in the Numerical Design of Optical Thin Film Systems", *Applied Optics*, (1982) **21**:8, pp.1502-1511.

[23] R. Serra, and G. Zanarini, *Complex Systems and Cognitive Processes*, (1990) Springer-

Verlag, New York.